Four-wave mixing in silicon-nanocrystal embedded high-index doped silica micro-ring resonator

Yuhua Li[1, 2], Xiang Wang[3], Roy Davidson[3], Brent E. Little[4], and Sai Tak Chu[2, †]

[1]Key Laboratory of Optical Field Manipulation of Zhejiang Province, Department of Physics, Zhejiang Sci-Tech University, Hangzhou 310018, China

[2]Department of Physics, City University of Hong Kong, Hong Kong 999077, China

[3]QXP Technology Inc., Xi'an 710119, China

[4]State Key Laboratory of Transient Optics and Photonics, XIOPM, CAS, Xi'an 710119, China

Abstract: A nonlinear integrated optical platform that allows the fabrication of waveguide circuits with different material composition, and at small dimensions, offers advantages in terms of field enhancement and increased interaction length, thereby facilitating the observation of nonlinear optics effects at a much lower power level. To enhance the nonlinearity of the conventional waveguide structure, in this work, we propose and demonstrate a microstructured waveguide where silicon rich layer is embedded in the core of the conventional waveguide in order to increase its nonlinearity. By embedding a 20 nm thin film of silicon nanocrystal (Si-nc), we achieve a twofold increase of the nonlinear parameter, γ. The linear relationship between the four-wave mixing conversion efficiency and pump power reveals the negligible nonlinear absorption and small dispersion in the micro-ring resonators. This simple approach of embedding an ultra-thin Si-nc layer into conventional high-index doped silica dramatically increases its nonlinear performance, and could potentially find applications in all-optical processing functions.

Key words: four-wave mixing; silicon nanocrystal; high-index doped silica; micro-ring resonator

1. Introduction

Highly nonlinear integrated waveguides play a key role in ultra-fast all-optical signal processing. A large number of nonlinear optics phenomena and applications have been demonstrated, in a variety of complementary metal–oxide–semiconductor (CMOS) compatible nonlinear integrated waveguides[1–11], as these integrated optical circuit platforms provide strong optical field confinement, thereby enhancing Kerr nonlinearity. To further enhance the nonlinearity of the integrated waveguides, a popular approach is to embed a highly nonlinear material, such as a silicon rich layer or a two-dimensional layer such as graphene[12, 13] in the waveguide. Although these silicon rich waveguides have higher nonlinearity, they also suffer from higher linear losses, resulting in a medium nonlinear figure-of-merit (FOM)[14]. Realizing both high nonlinearity and low propagation loss remain challenging. Low loss is essential in order to achieve compatibility with other linear elements in the circuit.

One platform that has drawn the attention of researchers in the field of nonlinear optics over the past decade involves the use of high-index doped silica glass[14–18]. The platform is CMOS-compatible with a mature fabrication process that is also suitable for mass production[14]. It features low linear and nonlinear losses, and is easily monolithically integrated with other linear components, so that both linear and nonlinear components can be fabricated on the same chip.

However, due to the lower index of the doped silica, it has a lower nonlinearity than silicon-rich platforms such as silicon and silicon nitride. It is therefore desirable to increase the nonlinearity of the doped silica platform, while maintaining its low loss property. We have discovered that by applying a strip of silicon-rich film, such as SiN, or a low dimensional high index layer such as silicon or silicon nanocrystal (Si-nc), in the core of the high-index doped silica waveguide, the nonlinearity can be increased to a large extent, resulting in only a slight alteration to the mode field distribution[19].

In this paper, a series of 49 GHz Si-nc embedded microring resonators (MRRs) are fabricated and their nonlinear properties characterized. The waveguide structure of the MRR consists of a thin layer of Si-nc, embedded in a high-index doped silica glass core. The main advantages of using Si-nc are its CMOS-compatiblility, relatively high nonlinearity, and negligible two-photon absorption (TPA)[20]. In the design of the waveguide structure, the dimension of the waveguide is optimized to achieve a stronger nonlinear interaction while keeping the propagation loss at a manageable level. In our experiment, we observe wavelength conversion from the four-wave mixing (FWM) process near 1550 nm under continuous-wave (CW) pump, at a power below 1 mW. The addition of a 20 nm thick Si-nc layer in the center of the core, results in a twofold increase in nonlinearity. CMOS-compatible integrated microchips with this modified structure have potential applications in high bandwidth optical communications.

2. Waveguide fabrication

Other than the deposition of a thin layer of Si-nc film in

Table 1.   Design parameters and fabrication processes of the MRRs.

Wafer	Structure	Anneal	a-Si deposition
w/o Si-nc layer	2 μm n = 1.60	4 h/1150 °C	–
w/ Si-nc layer	1 μm n = 1.60 + 50 nm Si-nc + RTA* @1100 °C 1 min + 1 μm n = 1.60	4 h/1150 °C	SiH$_4$ = 72 sccm, N$_2$O = 0, 349 W, 1 Torr, 5 s

*RTA: Rapid thermal annealing.

the middle of the core, the devices were fabricated using CMOS-compatible processes similar to those described in Refs. [14, 15, 21]. Plasma-enhanced chemical vapor deposition (PECVD) was employed in the deposition of the Si-nc embedded core waveguide films, beginning with a 1 μm n = 1.60 high-index doped silica layer on the SiO$_2$ lower cladding, followed by a ~ 50 nm thick amorphous silicon (a-Si) and finally another 1 μm n = 1.60 high-index doped silica layer to complete the deposition process. The deposited core film was then patterned, etched and clad with SiO$_2$ to form the waveguide. It is important to note that in addition to nonlinearity enhancement, the inclusion of an a-Si film will also increase the propagation and potentially TPA losses if its thickness is too great. On the basis of existing research into the dependency of the Si-nc layer location on waveguide nonlinearity and dispersion[19], we know that the level of nonlinear enhancement is highest when the Si-nc layer is positioned at the center of the core where the optical mode field is the strongest, however it will also induce the highest propagation loss. Although one can reduce the propagation loss by placing the Si-nc layer away from the center, e.g., on the surface of the waveguide core[22], this will also decrease its effect on nonlinear enhancement, and will require a longer waveguide to produce the same nonlinear effect. One advantage of placing the Si-nc film at the core center is that it enables the flattening of the waveguide dispersion, which is a highly desirable property in nonlinear applications. Along with the simulation of waveguide losses with different silicon rich materials[19], it has been found that a layer of 50 nm thick a-Si film located at the center of the core, results in optimal nonlinearity, loss and dispersion. To create the Si-nc film, the device was annealed at a high temperature to facilitate the crystallization of the a-Si film, and the formation of Si-nc grains. The size of Si-nc is dependent on the fabrication process, as well as the annealing conditions (atmosphere composition and temperature). The size and density of Si-nc can affect the effective index, which influences the nonlinear properties. Given that smaller Si-nc size tends to produce higher nonlinearity[23, 24], the objective is to control the production of Si-nc with respect to their dimension and size distribution. Design parameters and fabrication processes of different waveguides are shown in Table 1.

As the FWM conversion efficiency depends strongly on the Q-factor of the ring resonator, MRRs with different Q-factors are compared, so as to identify the maximum conversion efficiency of the Si-nc embedded waveguide structure. The Q-factor of the ring resonator can be varied by adjusting the gap separation between the bus waveguide and the ring. In our experiment, there are eight MRRs on one chip within a footprint of ~ 1 × 1 cm^2. In addition, MRRs with different dimensions are compared. For waveguides with a width of 2 μm, gap separations vary from 1.2 to 1.6 μm with a step of 0.1 μm, while for waveguides with a width of 3 μm, gap separations vary from 0.8 to 1.2 μm with a step of 0.2 μm. Further de-

Table 2.   Device parameters of the MRRs with a radius of 595 μm on the same mask.

No.	Gap (μm)	Width (μm)	Structure
D1	1.2	2	Add/drop
D2	1.3	2	Add/drop
D3	1.4	2	Add/drop
D4	1.5	2	Add/drop
D5	1.6	2	Add/drop
D6	0.8	3	Add/drop
D7	1.0	3	Add/drop
D8	1.2	3	Add/drop

tails of these parameters are listed in Table 2. Generally, larger waveguide cross-sections result in weaker mode distribution confinement, while propagation loss would be lower.

Transmission electron microscope (TEM) images of the annealed a-Si thin films reveal the Si-nc grain sizes and distributions throughout the whole wafer, and are shown in Fig. 1(a). From the TEM images we can conclude that after annealing under an N$_2$ atmosphere, Si-nc grains with a diameter of about 3 nm are obtained and the nanocrystal grains distribute uniformly across the wafer.

The designed cross-section geometries for Si-nc embedded waveguide are 2 × 2 μm^2 and 3 × 2 μm^2 with 50 nm Si-nc sandwiched in the core center. However, the cross-sectional dimensions of the as-deposited waveguides shrank by 13%–15% after the annealing process, as shown in the SEM images in Figs. 1(c) and 1(e). The actual dimensions of the two sets of waveguides are 1.75 × 1.75 μm^2 (w/20 nm Si-nc - D1) and 2.55 × 1.75 μm^2 (w/20 nm Si-nc - D6), respectively, with the thickness of the Si-nc layer being ~ 20 nm.

The mode profiles shown in Figs. 1(d) and 1(f) reveal that the electric field is tightly confined in the high-index doped silica core region. The zero-dispersion wavelengths of the transverse electric (TE) modes for the four waveguides are 1590 nm (w/o Si-nc - D6), 1520 nm (w/20 nm Si-nc - D6), 1520 nm (w/o Si-nc - D1), and 1340 nm (w/20 nm Si-nc - D1), respectively. With the exception of the waveguide with a cross-section of 2.55 × 1.75 μm^2 and without the Si-nc layer (w/o Si-nc - D6), all waveguides exhibit normal dispersion in the telecommunication window, due to the shrinkage of the cross-section, which shifted the dispersion towards the shorter wavelength direction. Normal dispersion will decrease the FWM conversion efficiency, but as our goal is to enhance the nonlinearity by introducing the Si-nc thin film, we can still compare our results among these waveguides. Moreover, for waveguides with marginally smaller normal dispersion, we demonstrate their applications in all-optical analog-to-digital conversion[25].

3. Intensity enhancement simulation

Optical intensity in the micro-ring is much higher than in the bus waveguide if the round-trip gain is larger than the
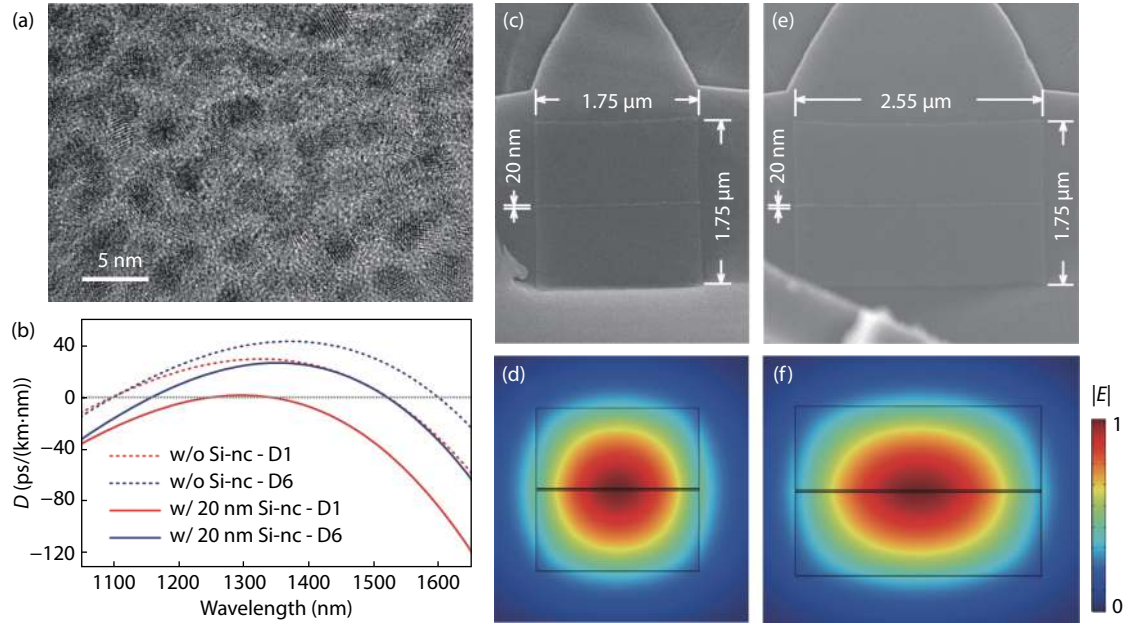
Fig. 1. (Color online) (a) TEM image of the Si-nc layer prior to deposition of the upper high-index doped silica layer. The sample was polished to an approximate 5 nm thickness for TEM characterization. (b) Computed dispersion of $1.75 \times 1.75\ \mu m^2$ (w/ 20 nm Si-nc - D1) and $2.55 \times 1.75\ \mu m^2$ (w/ 20 nm Si-nc - D6) cross-section for high-index doped silica waveguide embedded with 20 nm Si-nc, and without Si-nc case for cross-sections of $1.75 \times 1.75\ \mu m^2$ (w/o Si-nc - D1) and $2.55 \times 1.75\ \mu m^2$ (w/o Si-nc - D6). (c, e) SEM images of the fabricated Si-nc embedded waveguides. (d, f) Simulated electric field distribution of the fundamental TE mode of (c, e).
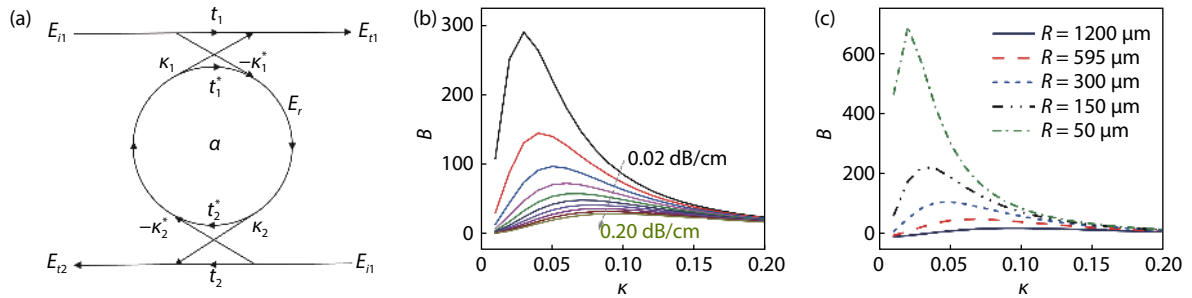

Fig. 2. (Color online) (a) Model of a basic add–drop single MRR[26]. (b) B versus κ for MRRs with the fixed radius of 595 μm while varying a in step of 0.02 dB/cm. (c) B versus κ with the fixed a of 0.1 dB/cm while varying the radius R.

loss. In an MRR with a configuration as shown in Fig. 2(a), the intensity enhancement factor B on resonance (with loss $a < 1$) is given by

$$B = \left| \frac{E_r}{E_{i1}} \right|^2 = \left| \frac{-\kappa_1^*}{1 - t_1^* t_2^* a} \right|^2, \qquad (1)$$

where κ and t are the coupling parameters of MRR. The * represents the conjugated complex value of κ and t. a denotes the loss coefficient in the micro-ring ($a = 1$ for zero loss).

The intensity enhancement factor B as a function of coupling coefficient κ was simulated for different propagation losses and various ring radii, results of which are presented in Figs. 2(b) and 2(c), respectively. Intensity enhancement in the ring is a function of round-trip loss and coupling coefficient. At a given round-trip loss, there is an optimal coupling coefficient located on the under coupled side of the critical coupling point, where the intensity enhancement is at its maximum. For a lossless resonator, intensity enhancement factor B is equal to the inverse of the power coupling coefficient. As a function of radius, enhancement increases with decreased radi-

us. This is due mainly to the reduction of the mode volume and round-trip loss. Enhancement B can increase Kerr nonlinearity, which is beneficial in nonlinear processes, such as FWM.

4. Waveguide characterization

The linear properties of the fabricated ring resonators with the conventional waveguide structure are shown in Table 3 and for the MRRs with the Si-nc waveguide in Table 4. It can be seen that the loaded Q-factors for both the conventional and the Si-nc embedded MRRs increase as a function of gap separation from 1.2 to 1.6 μm for the $1.75 \times 1.75\ \mu m^2$ MRRs and from 0.8 to 1.2 μm for the $2.55 \times 1.75\ \mu m^2$ MRRs, indicating that the MRRs are not loss limited. With the field enhancement factor in the resonator proportional to its finesse, the amount of stored power in the resonator is higher for resonators with a higher Q value, for a given input power. However, as the gap separation increases, the Q value will saturate once the intrinsic loss is larger than the coupling between the resonator and the bus waveguide. At

Table 3. Measured parameters for devices without Si-nc layer.

No.	Cross-section (μm^2)	Gap (μm)	κ_1, κ_2	α (dB/cm)	Q (TE)	FSR	B
D1	1.75×1.75	1.2	0.1063	0.11	7.4×10^5	49	27.3
D2	1.75×1.75	1.3	0.0818	0.11	1.0×10^6	49	26.2
D3	1.75×1.75	1.4	0.0667	0.10	1.3×10^6	49	25.7
D4	1.75×1.75	1.5	0.0541	0.14	1.3×10^6	49	12.8
D5	1.75×1.75	1.6	0.0417	0.13	1.8×10^6	49	11.5
D6	2.55×1.75	0.8	0.1007	0.08	8.6×10^5	49	35.9
D7	2.55×1.75	1.0	0.0687	0.08	1.5×10^6	49	38.3
D8	2.55×1.75	1.2	0.0524	0.05	2.5×10^6	49	57.3

Table 4. Measured parameters for devices with 20 nm Si-nc layer.

No.	Cross-section (μm^2)	Gap (μm)	κ_1, κ_2	α (dB/cm)	Q (TE)	FSR	B
D1	1.75×1.75	1.2	0.1324	0.15	4.9×10^5	49	30.4
D2	1.75×1.75	1.3	0.0995	0.20	6.3×10^5	49	28.8
D3	1.75×1.75	1.4	0.0833	0.19	7.8×10^5	49	30.4
D4	1.75×1.75	1.5	0.0542	0.32	7.2×10^5	49	10.8
D5	1.75×1.75	1.6	0.0504	0.27	8.6×10^5	49	13.1
D6	2.55×1.75	0.8	0.1325	0.18	4.6×10^5	49	27.5
D7	2.55×1.75	1.0	0.0783	0.15	9.5×10^5	49	40.1
D8	2.55×1.75	1.2	0.0497	0.16	1.3×10^6	49	28.7

that point, the power in the resonator decreases and the efficiency will subsequently decrease. With increasing gap separation, Q increases, while κ and B decrease. With increasing waveguide width, Q value increases, while κ, α and B decrease. Intensity enhancement factor B is obtained by fitting the curve of the through port and the drop port. As the thickness of the Si-nc film is more than an order of magnitude smaller than the wavelength, it has almost no effect on the effective index of the MRRs so that the FSRs of the MRRs with and without the Si-nc layers are similar.

The coupling coefficients κ_1, κ_2, and the propagation loss in the ring α in Tables 3 and 4 are extracted from the measured responses by fitting the measured responses with the analytical formulas[27]. At 1550 nm, the extracted propagation loss of the ring embedded with 20 nm Si-nc strip is ~ 0.1 dB/cm higher than for a case without the strip. The α values of these two wafers are below 0.32 dB/cm. Although the low propagation loss in the ring indicates the promise of these devices for use in nonlinear experiments, it is important to point out that as the Q-factor of the MRR is highly dependent on the propagation loss, the increased loss with the additional layer of Si-nc film reduces the Q-factor of the MRRs by a factor of approximately half. Furthermore, due to the high propagation loss of transverse magnetic (TM) polarization, we only study the linear and nonlinear properties of TE polarization.

The fiber to waveguide coupling loss for the MRRs devices is around 5 dB/facet. Figs. 3(a)–3(d) show the measured responses from through port and drop port across the C-band for TE mode of the 49 GHz FSR. The 3 dB bandwidth for the four waveguides from Fig. 3(e) to Fig. 3(h) is 269, 288, 367, and 379 MHz, respectively.

5. Results and discussions

The nonlinear parameter γ was measured for the 49 GHz MRRs, based on the conversion efficiency η of the FWM process, with the field enhancement from the micro-

ring also taken into consideration, in accordance with[15, 28]:

$$\eta \equiv \frac{P_{idler}}{P_{signal}} = |2\pi R\gamma|^2 P_{pump}^2 \cdot (FE_p)^4 \cdot (FE_s)^2 \cdot (FE_i)^2, \quad (2)$$

$$FE_\mu = \frac{\sqrt{2(1 - t_\mu)}}{2(1 - t_\mu) + \alpha_\mu \pi R}, \quad (3)$$

$$t_\mu = \left(1 - \frac{\pi}{2F_\mu}\right) \exp\left(\frac{\alpha_\mu \pi R}{2}\right), \quad (4)$$

where R denotes the radius of the MRR. Here, FE_p, FE_s and FE_i represent the field enhancement at the pump, signal and idler wavelengths, respectively. The product $(FE_p)^4 \cdot (FE_s)^2 \cdot (FE_i)^2$ corresponds to the overall power enhancement of the MRR. α_μ is the mode linear loss of the μ-th order of the mode. t_μ is the self-coupling coefficient between the bus waveguide and the ring. F_μ is the finesse of the MRR filter, which is given by the ratio of FSR and 3 dB width for the mode μ. Using the MRRs, we measured the nonlinear parameter γ by exciting the pump and the signal power from the input and add ports, respectively[15]. Pump and signal wavelengths are tuned carefully to align with two resonances to utilize the maximum cavity enhancement.

When a laser with high pump power is launched into the waveguide, the generated heat will shift the resonances. Thermal shift rate of the high-index doped silica glass is approximately 17 pm/°C at 1550 nm[29]. Taking into account the fact that cold resonance can shift to longer wavelength by almost a half-line width with a temperature change of as little as 0.1 °C[30], we use a thermoelectric cooler (TEC) stage with thermocouple feedback to maintain thermal balance, as shown in Fig. 4(a). Both the drop and the through responses are measured using the same OSA with the aid of an optical switch.

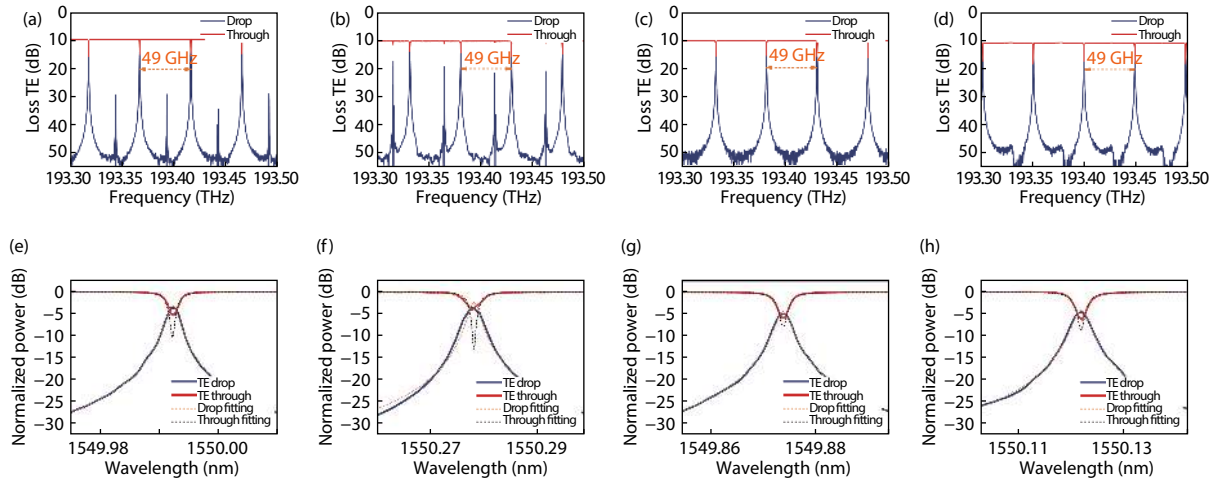The generated first and second idler signals from the

Fig. 3. (Color online) Optical response of TE mode from the through port and drop port of 49 GHz MRRs with (a, e) cross-section of 1.75 × 1.75 μm² without Si-nc layer, (b, f) cross-section of 2.55 × 1.75 μm² without Si-nc layer, (c, g) cross-section of 1.75 × 1.75 μm² with 20 nm Si-nc, and (d, h) cross-section of 2.55 × 1.75 μm² with 20 nm Si-nc.
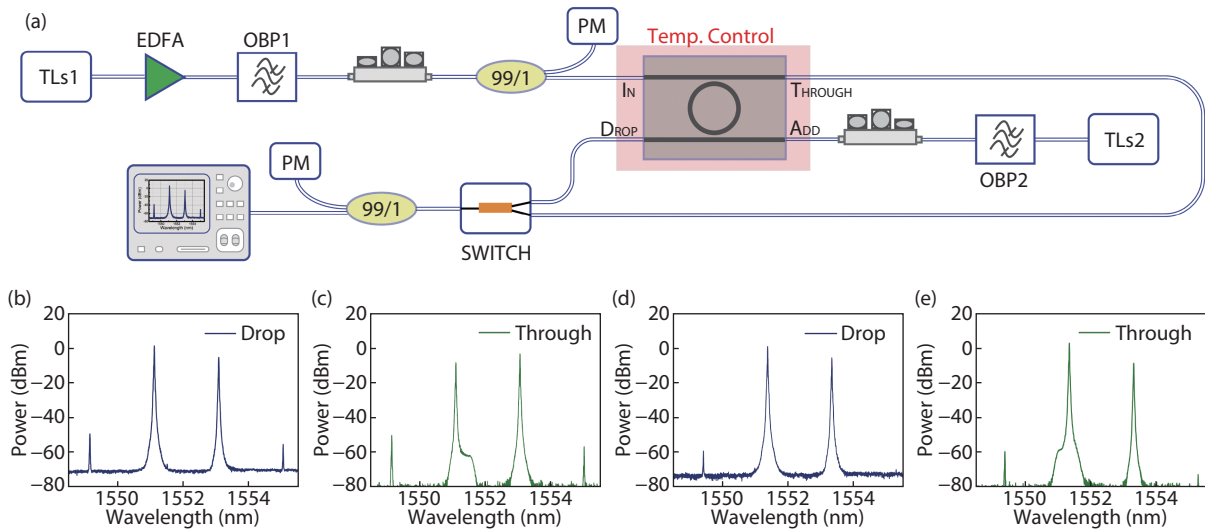

Fig. 4. (Color online) (a) Experimental setup for FWM process. (b–e) Recorded spectra from OSA of MRRs with cross-section of 1.75 × 1.75 μm² (b, c) without Si-nc layer, and (d, e) with 20 nm Si-nc layer.

FWM process in the MRRs are shown in Figs. 4(b)–4(e). When aligning the pump and signal wavelengths with the resonances, idler peaks can be recorded on both sides with the frequencies satisfying the energy conservation $\omega_{idler1} = 2\omega_{pump} - \omega_{signal}$ or $\omega_{idler2} = 2\omega_{signal} - \omega_{pump}$. The recorded idler peaks are all aligned on resonances, indicating that the dispersion at these wavelengths is negligible.

We note that while both the 1.75 × 1.75 μm² and 2.55 × 1.75 μm² MRRs have similar Q-factors, but the 1.75 × 1.75 μm² MRR has a higher FWM converson efficiency due to the higher power density, shown in Fig. 5(a). The measured nonlinear parameter γ extracted from the FWM measurement for the MRRs is shown in Table 5. It can be seen that γ increased from 0.144 to 0.366 W^{-1}m^{-1} for the 1.75 × 1.75 μm² MRR and from 0.120 to 0.212 W^{-1}m^{-1} for the 2.55 × 1.75 μm² MRR with the addition of the Si-nc film. The increase of the nonlinear parameter γ by adding the Si-nc film is with the tradeoff of additional propagation loss, resulting in a lower Q-factor and intensity enhancement of the MRRs, which results in the low FWM conversion efficiency. Fig. 5(b) plots the linear relationship of the idler power versus the square of the pump power and reveals a quadratic dependence, demonstrating that the Si-nc film exhibits no TPA and 3PA absorption under input pump powers up to 15 mW, and which is limited by the available CW pump source. Moreover, using long path length spiral waveguides with the same embedded Si-nc thin film, we observed that the TPA is negligible, derived from measured reciprocal transmission as a function of the coupled peak power[25].

6. Conclusions

In conclusion, we have fabricated a series of 49 GHz MRRs with embedded Si-nc layers and measured their FWM efficiency. The Si-nc film is formed by the deposition of a thin layer of a-Si film in the middle of the core waveguide, and subsequently crystallized at a high temperature. We found that the addition of the Si-nc film increased the propagation loss by approximately 0.11 to 0.15 dB/cm and reduced the Q-factor of the MRRs by one half, however the Si-nc film doubles the nonlinear parameter γ. By adding a thin layer of
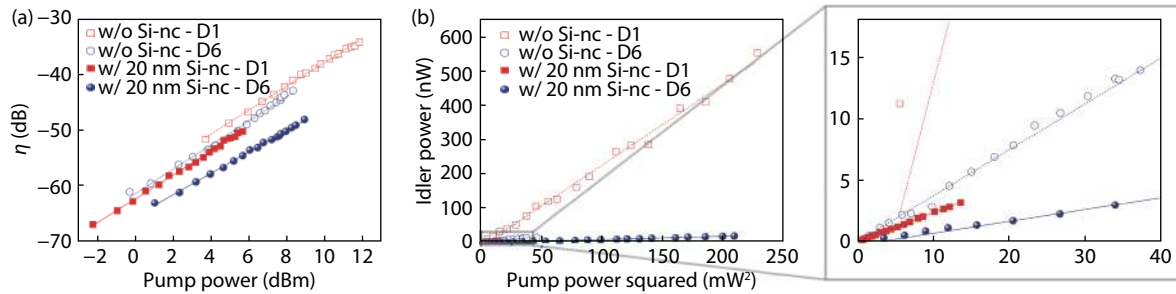
Fig. 5. (Color online) (a) Conversion efficiency versus incident pump power for FWM in the 49 GHz MRRs for with and without Si-nc thin film cases. (b) Idler power dependence of the square of the pump power for FWM in the MRRs for with and without Si-nc thin film cases.

Table 5.   Parameter comparisons of the 49 GHz MRRs for dominant TE polarization.

Wafer	No.	Cross-section (μm^2)	Insertion loss (dB/facet)	$(FE_p)^4(FE_s)^2(FE_i)^2$	γ ($W^{-1}m^{-1}$)
w/o Si-nc layer	D1	1.75×1.75	4.8	5.6×10^6	0.144
w/o Si-nc layer	D6	2.55×1.75	5.1	4.6×10^6	0.120
w/ 20 nm Si-nc layer	D1	1.75×1.75	5.0	3.4×10^5	0.366
w/ 20 nm Si-nc layer	D6	2.55×1.75	5.4	4.1×10^5	0.212

Si-nc film, it is possible to enhance the nonlinearity of the waveguide and to improve these waveguide circuits for all optical signal processing applications.

Acknowledgments

References

[1]   Lin S Y, Schonbrun E, Crozier K. Optical manipulation with planar silicon microring resonators. Nano Lett, 2010, 10, 2408

[2]   Lin Q, Zhang J, Piredda G, et al. Dispersion of silicon nonlinearities in the near infrared region. Appl Phys Lett, 2007, 91, 021111

[3]   Shoji Y, Ogasawara T, Kamei T, et al. Ultrafast nonlinear effects in hydrogenated amorphous silicon wire waveguide. Opt Express, 2010, 18, 5668

[4]   Ikeda K, Saperstein R E, Alic N, et al. Thermal and Kerr nonlinear properties of plasma-deposited silicon nitride/silicon dioxide waveguides. Opt Express, 2008, 16, 12987

[5]   Guo H R, Herkommer C, Billat A, et al. Mid-infrared frequency comb via coherent dispersive wave generation in silicon nitride nanophotonic waveguides. Nat Photonics, 2018, 12, 330

[6]   Brasch V, Geiselmann M, Herr T, et al. Photonic chip–based optical frequency comb using soliton Cherenkov radiation. Science, 2016, 351, 357

[7]   Karpov M, Pfeiffer M H, Guo H R, et al. Dynamics of soliton crystals in optical microresonators. Nat Phys, 2019, 15, 1071

[8]   Bao H L, Cooper A, Rowley M, et al. Laser cavity-soliton microcombs. Nat Photonics, 2019, 13, 384

[9]   Corcoran B, Tan M X, Xu X Y, et al. Ultra-dense optical data transmission over standard fibre with a single chip source. Nat Commun, 2020, 11, 2568

[10]   Singh N, Raval M, Ruocco A, et al. Broadband 200-nm second-harmonic generation in silicon in the telecom band. Light Sci Appl, 2020, 9, 17

[11]   Wang F X, Wang W Q, Niu R, et al. Quantum key distribution with on-chip dissipative kerr soliton. Laser Photonics Rev, 2020, 14, 1900190

[12]   Lin H T, Song Y, Huang Y Z, et al. Chalcogenide glass-on-graphene photonics. Nat Photonics, 2017, 11(12), 798

[13]   Zhao Y, Lu J, Huo Y Y, et al. Enhanced third harmonic generation from graphene embedded in dielectric resonant waveguide gratings. Opt Commun, 2019, 447, 30

[14]   Moss D J, Morandotti R, Gaeta A L, et al. New CMOS-compatible platforms based on silicon nitride and Hydex for nonlinear optics. Nat Photonics, 2013, 7, 597

[15]   Ferrera M, Razzari L, Duchesne D, et al. Low-power continuous-wave nonlinear optics in doped silica glass integrated waveguide structures. Nat Photonics, 2008, 2, 737

[16]   Ferrera M, Park Y, Razzari L, et al. On-chip CMOS-compatible all-optical integrator. Nat Commun, 2010, 1, 29

[17]   Razzari L, Duchesne D, Ferrera M, et al. CMOS-compatible integrated optical hyper-parametric oscillator. Nat Photonics, 2010, 4, 41

[18]   Pasquazi A, Peccianti M, Park Y, et al. Sub-picosecond phase-sensitive optical pulse characterization on a chip. Nat Photonics, 2011, 5, 618

[19]   Wei P, Wang S, Little B E, et al. Analysis of a Si-nanocrystal strip-loaded waveguide for nonlinear applications. International Conference on Photonics in Switching (PS), 2016

[20]   Martínez A, Hernández S, Lebour Y, et al. Two-photon absorption in Si-nanocrystals deposited by plasma-enhanced chemical-vapor deposition. Physica E, 2009, 41, 1002

[21]   Little B. A VLSI photonics platform. Optical Fiber Communications Conference, 2003, 444

[22]   Wu J, Yang Y, Qu Y, et al. 2D layered graphene oxide films integrated with micro-ring resonators for enhanced nonlinear optics. Small, 2020, 16, 1906563

[23]   Sanchis P, Blasco J, Martinez A, et al. Design of silicon-based slot waveguide configurations for optimum nonlinear performance. J Lightwave Technol, 2007, 25, 1298

[24]   Spano R, Daldosso N, Cazzanelli M, et al. Bound electronic and free carrier nonlinearities in Silicon nanocrystals at 1550 nm. Opt Express, 2009, 17, 3941

[25]   Li Y H, Zhu K, Kang Z, et al. CMOS-compatible high-index doped silica waveguide with an embedded silicon-nanocrystal strip for

all-optical analog-to-digital conversion. Photon Res, 2019, 7, 1200

[26] Rabus D G, Sada C. Sensors. Integrated Ring Resonators. Cham: Springer International Publishing, 2020, 293

[27] Little B E, Chu S T, Haus H A, et al. Microring resonator channel dropping filters. J Lightwave Technol, 1997, 15, 998

[28] Absil P P, Hryniewicz J V, Little B E, et al. Wavelength conversion in GaAs micro-ring resonators. Opt Lett, 2000, 25, 554

[29] Little B E, Chu S T, Absil P P, et al. Very high-order microring resonator filters for WDM applications. IEEE Photonics Technol Lett, 2004, 16, 2263

[30] Ferrera M, Duchesne D, Razzari L, et al. Low power four wave mixing in an integrated, micro-ring resonator with Q = 1.2 million. Opt Express, 2009, 17, 14098

Yuhua Li received the PhD degree in Applied Physics from City University of Hong Kong in 2020. Since December 2020 she has been with Zhejiang Sci-Tech University where she is currently a full lecturer. Her current research interests include nonlinear optics, integrated photonic device, and luminescent rare-earth ions.

Sai Tak Chu received the PhD degree in Electrical Engineering from the University of Waterloo in 1990. He joined the City University of Hong Kong in 2010 where he is currently an Associate Professor in the Department of Physics. His current research interests include linear and nonlinear integrated optical circuits.